Oxidation of Metals, Vol. 3, No. 5, 1971

Oxidation Behavior of Ni–Cr–1ThO_2 Alloys at 1000 and 1200°C

H. H. Davis,* H. C. Graham,* and I. A. Kvernes†

Received May 4, 1971—Revised May 14, 1971

The oxidation behavior of Ni–13.5–33.7Cr–1ThO_2 alloys in flowing oxygen at 150 Torr was investigated in the temperature range 1000–1200°C. Gravimetric measurements of the oxidation kinetics have been combined with microstructural studies of the reacted samples in order to evaluate the reaction mechanisms. The oxide products formed on the alloys were a function of Cr content, sample surface preparation, reaction time, and temperature. The presence of ThO_2 appears to produce two effects during alloy oxidation. First, enhanced Cr diffusion to the alloy surface results in rapid formation of a Cr_2O_3 subscale beneath NiO on Ni–13.5Cr–1ThO_2 and selective oxidation of Cr for Ni–22.6Cr–1ThO_2. Second, the mechanism of formation of Cr_2O_3 is apparently different from that for simple Ni–Cr alloys, resulting in about an order of magnitude reduction in the Cr_2O_3 growth rate. The oxidation–vaporization of Cr_2O_3 to CrO_3 becomes rate controlling for the higher Cr alloys after only a few hours of exposure at 1200°C.

INTRODUCTION

Researchers in the area of alloy development are continually striving to obtain materials which possess good strength and creep resistance at elevated temperatures. Such efforts have led in recent years to the development of dispersion-strengthened alloys, which exhibit both a resistance to recrystallization at temperatures near the melting point of the matrix metal and a stress-rupture response which is nearly temperature independent. The first commercial dispersion-strengthened Ni-base alloy was thoriated Ni, which is strengthened by submicron ThO_2 particles uniformily distributed throughout the microstructure. However, the oxidation behavior of this

*Aerospace Research Laboratories, Wright–Patterson AFB, Ohio.
†Central Institute for Industrial Research, Oslo-Blindern, Norway.

alloy does not differ substantially from that of pure Ni, thus requiring that it be coated for elevated temperature use. As a result, Cr has been added as an alloying addition to improve the high temperature oxidation resistance. An additional effect of Cr is to reduce the high temperature steady-state creep rate.[1]

The mole fraction of Cr which must be present in a thoriated Ni–Cr alloy to ensure selective oxidation of Cr is uncertain. In binary Ni–Cr alloys, approximately 30 wt.% Cr is required[2] for selective oxidation to occur at 0.1 atm oxygen. Also uncertain is whether the ThO_2 particles remain inert with respect to the oxidation reactions, or whether they influence the oxidation behavior. In a review paper, Rapp[3] has reported that dispersion-strengthened metals similar to thoriated Ni exhibit oxidation behavior which differs very little from that of the matrix metal. Other types of metal–particle combinations were shown to affect the oxidation resistance. The purpose of the present paper is to report the results of the oxidation of thoriated Ni–Cr alloys containing different Cr contents, and to determine if the presence of ThO_2 particles affects the oxidation behavior.

EXPERIMENTAL PROCEDURE

Thoriated alloys containing different Cr contents (alloy I, 13.5 wt. %; alloy II, 22.6 wt.%; alloy III, 33.7 wt.%) were prepared by Sherritt Gordon Mines, Ltd. as an experimental batch process. The preparation procedure and alloy characterization, including complete chemical analyses, have been reported elsewhere,[1] and are summarized here.

Billets, obtained by powder metallurgical techniques, were cross rolled into sheet with intermediate anneals in H_2 at 1200°C. Final sheet thickness was approximately 0.021 in., and a final anneal at 1200°C in H_2 was carried out for 30 min. Primary impurities include Fe, Co, and Al. In general, the alloys are similar with respect to size and distribution of the ThO_2 particles, amount of recrystallization, and grain size, but they were not found to have a homogeneous Cr distribution. The ThO_2 content is about 1.1 wt.% in all the alloys. A characteristic of the higher Cr content alloys was the presence of a thin oxide scale and oxide pits prior to any intentional oxidation treatment. As described below, these were removed by grinding prior to oxidation testing.

The as-received sheet was sheared into square coupons with sides of approximately 1 cm length. At least 0.001 in. was removed from each side of the samples by conventional wet grinding techniques through 600 grit SiC abrasive. This procedure constituted one surface preparation technique used in this study and is referred to as "abraded." As a second surface preparation, the grinding procedure was followed by mechanical polishing

of the surface on a wet lap using No. 2 Al_2O_3 and is called "polished." In both cases, the samples were cleaned with alcohol prior to being oxidized.

Continuous gravimetric measurements were carried out during alloy oxidation using a Cahn RG electrobalance. Samples were lowered directly into the pure oxygen environment at the test temperature using techniques which have been described in detail previously.[4] Oxidation times varied from 5 min to 150 hr, but were usually 20 to 50 hr in duration. The pure oxygen continuously flowed past the sample at an average linear flow rate of 12 cm/sec (forced convection). This is equivalent to a volumetric flow rate of 254 cm^3/sec being directed into the system at a pressure of 1 atm. The pressure in the reaction chamber was maintained at 150 Torr.

After oxidation, specimens were removed directly from the oxidizing environment and the scales were x-rayed *in situ* at room temperature. Additionally, any oxide products which spalled from the sample during oxidation or cooling were collected in an alumina dish at the bottom of the reaction chamber. Such flakes were also subjected to x-ray analysis. In some cases when thick oxide scales formed, x-ray diffraction analyses were performed following successive grinding steps through the oxide layers. Oxidized samples were cut and mounted for metallographic observation of their cross sections. Both electron microprobe studies of elemental distribution and scanning electron microscopy of oxide topography were performed.

RESULTS AND DISCUSSION

Alloy Homogeneity

Electron microprobe line traces were carried out on metallographically prepared specimens in the as-received condition to determine the uniformity of the Cr distribution. Traces were performed both across the sheet thickness and parallel to the sheet surface at a distance of approximately 30 μ from the surface. Inhomogeneities in the Cr distribution, particularly for alloy I, were observed. In the extreme case, the Cr content varied from 13.5 to 18.5 wt.% across the sheet thickness. These inhomogeneities in the as-received alloy caused variations in the oxidation products on opposite sides of abraded specimens of alloy I oxidized at 1200°C. For polished specimens of alloy I, there was no difference in the oxidation products on opposite sides of the sheet, consequently the Cr variation is thought to have produced no significant effect. For alloys II and III, the Cr inhomogeneities have little importance since the initial Cr content is sufficient to produce selective oxidation over the entire specimen.

Alloy I was further observed to contain a preferred grain orientation on the sheet side having the lower Cr content. This deformation texture was

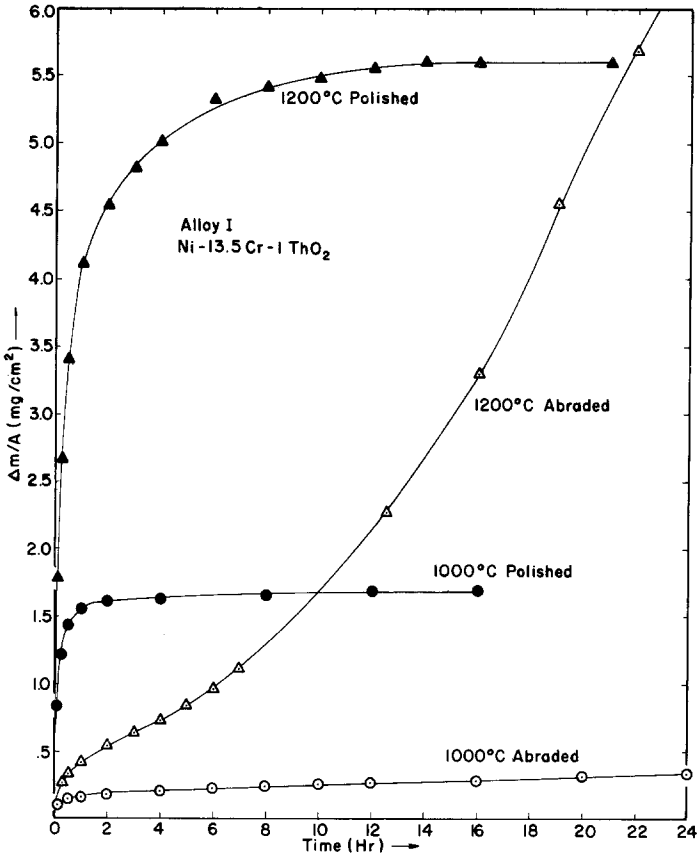

Fig. 1. Typical oxidation kinetics for Ni–13.5Cr–1ThO_2 at 1000 and 1200°C. Note the effect of surface preparation on growth kinetics.

such that the (220) plane was approximately parallel to the sheet surface. Random orientation of the grains was observed on the higher Cr side.

Alloy I Oxidation Behavior

Typical weight change *vs.* time curves for Ni–13.5Cr–1ThO_2 are presented in Fig. 1. These data are plotted on a linear scale since, in general, the behavior does not follow a particular rate law (such as parabolic). For this alloy, polished samples are observed to oxidize at a more rapid initial rate than those which were abraded. This larger initial weight gain was followed by a period of very little weight change.

During the period of rapid weight gain, NiO grows as the main reaction product at both 1000 and 1200°C. However, x-ray diffraction results also

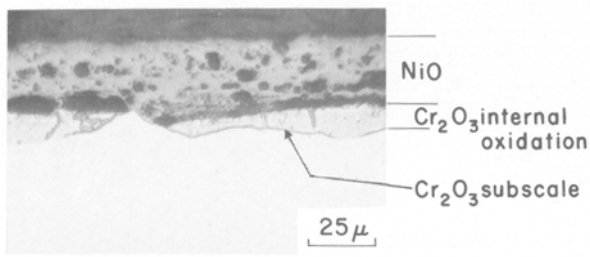

Fig. 2. Oxide scale morphology for polished specimen of Ni–13.5Cr–1ThO_2 following 20 min exposure at 1200°C. Note zone of internal oxidation particles and portions of continuous Cr_2O_3 subscale.

show both Cr_2O_3 and $NiCr_2O_4$ spinel to be present in small quantities. The NiO grows as double-layer type scale, with a region of Cr_2O_3 at the NiO–alloy interface. Both spinel and Cr_2O_3 particles are probably located in the inner layer of the NiO scale. Spinel is usually formed as the solid-state reaction product between NiO and Cr_2O_3.

Figure 2 illustrates the region of Cr_2O_3 which forms at the NiO–alloy interface for short oxidation times. A band of discrete Cr_2O_3 particles, commonly referred to as internal oxidation,[5] occurs beneath the NiO scale. Outlining the edges of the internal oxidation region are portions of a continuous Cr_2O_3 subscale or healing layer, the growth of which may follow grain boundaries in the alloy.

As oxidation of the alloy proceeds, Cr_2O_3 subscale regions join together to form a continuous Cr_2O_3 healing layer. The Ni-rich metal surrounding the internal oxide particles then oxidizes to form NiO, resulting in a scale morphology illustrated in Fig. 3: a double layer NiO and a continuous

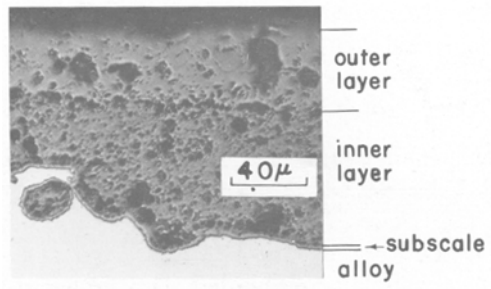

Fig. 3. Oxide scale morphology for polished specimen of Ni–13.5Cr–1ThO_2 following 46-hr exposure at 1200°C. Continuous Cr_2O_3 subscale has formed beneath double-layer NiO scale.

Cr_2O_3 subscale at the NiO–alloy interface. Once formed, this scale morphology remains intact throughout the duration of oxidation exposure.

The development of the Cr_2O_3 subscale generates the kinetic behavior shown for polished samples in Fig. 1. The initial rapid weight gain corresponds to the formation and growth of the two-layer NiO scale. Simultaneously, the Cr_2O_3 internal oxidation particles are coalescing along alloy–grain boundaries near the oxide–alloy interface. Once the Cr_2O_3 has formed a continuous subscale over the entire alloy and oxidation of the metal matrix within the zone of internal oxide particles is complete, the oxidation rate is then controlled by diffusion through the Cr_2O_3 layer. The associated reduced oxidation rate is revealed by the sharp decrease in the rate of weight gain as indicated in Fig. 1.

An additional feature observed in Fig. 1 is that the decrease in oxidation rate occurs at a shorter time at 1000°C than at 1200°C, which may indicate that the Cr_2O_3 subscale becomes continuous more rapidly at 1000 than at 1200°C. These results are viewed with caution since the inhomogeneous Cr distribution leads to poor quantitative reproducibility of results for this alloy.

The results have shown that polished samples of alloy I after extended oxidation times form a double layer or duplex type NiO scale with a thin, compact Cr_2O_3 subscale. The literature[6–12] contains numerous reports relating to the mechanism of formation of duplex NiO scales on Ni and on dilute Ni–Cr alloys. The most accepted mechanism relates to the partial dissociation of the initially formed NiO at the alloy–oxide interface, producing atomic oxygen which then diffuses into the alloy to form Cr_2O_3 precipitates internally. When a dilute Ni–Cr alloy is exposed to oxygen, both NiO and Cr_2O_3 may form initially, but these rapidly combine to produce $NiCr_2O_4$ particles in a saturated solution of Cr in NiO.[9] Since NiO is a cation-deficient metal oxide, new scale is formed at the oxide–gas interface by the outward diffusion of cations so long as the metal–scale interface maintains intimate contact. However, loss of intimate contact may occur by either (1) insufficient plasticity in the growing oxide layer or by (2) condensation of cation vacancies into the metal–scale interface to create voids. The local supply of metal is restricted at the void, resulting in a decrease in the local Ni activity in the oxide layer while a corresponding increase in the local oxygen activity occurs by additional oxygen uptake at the oxide–gas interface. Consequently, the oxide adjacent to the voids tends to dissociate into Ni^{2+} ions and oxygen molecules. Metal atoms react directly with the oxygen gas present in the void, and a porous inner oxide scale is initiated and grows in this manner. Thus, both the inner and the outer layers thicken with time, with their growth modes and directions being different. The porous, inner layer thickens by the inward growth of NiO through the

arrival of oxygen molecules, and the outer NiO layer grows by the outward diffusion of Ni^{2+} ions to react at the outer surface. These cations are supplied by both the dissociation process and cation diffusion across the inner NiO scale. The interface between the compact outer scale and the porous inner layer approximates the original alloy surface.[13]

As the inner NiO layer advances into the alloy matrix, it engulfs the Cr_2O_3 internal oxide particles. These particles are then slowly converted into $NiCr_2O_4$ spinel particles of the same general morphology by solid state reaction between NiO and Cr_2O_3.

The presence of the dispersed ThO_2 particles in the alloy assures the rapid initiation of the dissociation mechanism.[3] At the metal–scale interface, the ThO_2 particles locally screen the chemical bonding forces which are responsible for maintaining intimate contact between the metal and the scale. Thus, voids are introduced immediately after the start of the oxidation reaction, followed by the formation and growth of the duplex-type NiO scale.

For binary Ni–Cr alloys, Giggins and Pettit[2,14] have shown that the Cr_2O_3 internal oxidation particles do not coalesce to form a continuous subscale until the Cr content in the alloy reaches 20 wt.%. For Ni–15Cr and Ni–10Cr, however, Cr_2O_3 did form as continuous subscales along alloy grain boundaries. It therefore appears that bulk diffusion of Cr through alloy grains is too slow with respect to the rate of formation of the zone of internal precipitation to produce the necessary volume fraction of Cr_2O_3 to develop a continuous subscale on Ni–15Cr. Some disagreement exists in the literature as to whether continuous Cr_2O_3 subscales form on Ni–10Cr alloys.[15] In studies[16,17] currently under way, internal oxidation of Cr is observed on Ni–10Cr at 1000°C, but the addition of 0.5Y to the alloy favors formation of a continuous subscale. As pointed out by Giggins and Pettit,[2] these apparent divergences in the results may be attributed to differences in grain size at the surfaces of the unoxidized alloys.

In the present study, a continuous subscale was observed to form on the Ni–13.5Cr–1ThO_2 alloy within a few hours of exposure at 1000 and 1200°C. This suggests that enhanced Cr diffusion is occurring throughout the alloy matrix. Fleetwood[18] has reported that the diffusivity of chromium in a Ni–5ThO_2 alloy is substantially greater than that in nickel. Enhanced diffusion in thoriated Ni is attributed to the microstructure which is developed in this alloy. The fine dispersion of thoria particles stabilizes a fine subgrain structure which persists at temperatures up to 1200°C. Thus, at temperatures where unthoriated Ni or simple Ni–Cr alloys would experience rapid grain growth, the high density of subgrain boundaries and associated dislocations in thoriated alloys affords short-circuit diffusion paths which increase diffusion rates.

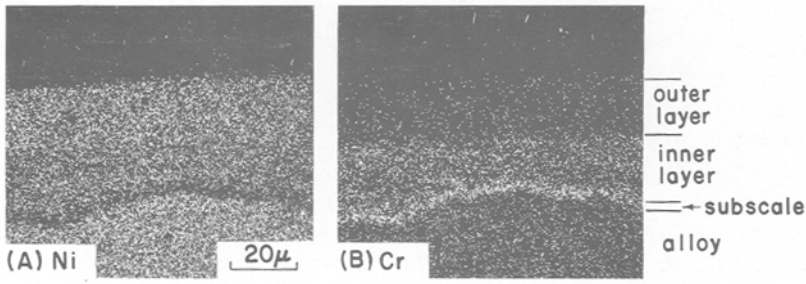

Fig. 4. Microprobe x-ray images taken from polished specimen of Ni–13.5Cr–1ThO_2 following 4-hr exposure at 1200°C.

Characterization of the microstructure and substructure of the as-received alloys used in this study has been reported by Wilcox and Clauer.[1] While some grain extension persists in the direction of working, the microstructure is considered to be recrystallized since annealing twins are observed within the grains. In addition, a dislocation substructure is observed to be present in the alloys, with the individual dislocations being strongly pinned by the dispersed ThO_2 particles. In agreement with the findings of Fleetwood,[18] the annealing twins and high dislocation density are apparently sufficient to provide the short-circuit diffusion paths which are responsible for the rapid formation of the continuous Cr_2O_3 subscales on polished specimens of alloy I.

Figure 4 shows microprobe x-ray images of the oxide scale region for a specimen of alloy I which was oxidized for 4 hr at 1200°C. Both the NiO duplex scale and the Cr_2O_3 continuous subscale are revealed by these scans. Furthermore, Cr is distributed throughout both regions of the NiO duplex scale. Quantitative determinations from the electron microprobe reveal that the Cr concentration is typically 15–20 wt.% in the inner NiO layer. In the outer layer, the Cr content varied from about 1% at the oxide–gas interface to 3% at the NiO outer–inner scale interface. Wood and Hodgkiess[9] reported the Cr concentration at the NiO inner layer–outer layer interface to be consistently 3.5–4.5% for a range of dilute Ni–Cr alloys, suggesting that the solubility of Cr in NiO was being satisfied there. For Ni–14.6Cr oxidized at 1000°C, Wood and Hodgkiess[10] obtained a nearly uniform value of 20–22% Cr in the inner NiO layer for many specimens, which they attributed to NiO and $NiCr_2O_4$ in a weight ratio of 1:1, or NiO and Cr_2O_3 in a ratio of 2:1, or a mixture of all three phases.

X-ray images for Th corresponding to Fig. 4 did not show regions of varying Th concentration. However, in a study of the oxidation behavior of Ni–2ThO_2 from 900 to 1400°C, Pettit and Felten[12] observed the growth of a

duplex NiO scale, with thoria particles being located in the inner layer but not in the outer oxide. They also reported no indication of mutual solubility or reaction between NiO and ThO_2 at 1400°C. The oxidation rate of Ni–2ThO_2 from 600 to 1000°C was reported by Jones and Westerman[19] to be less than that of pure Ni, but no determination of thorium in the oxide scale was made. Unpublished work[20] on the oxidation of Ni–1ThO_2 is in agreement with the findings of Pettit and Felten, with no thorium concentration being observed in the outer scale. According to the mechanism by which the duplex NiO scale forms, the outer layer grows by outward cation diffusion with reaction at the oxide–gas interface. Consequently, the ThO_2 particles would not be expected to be present in the outer NiO layer.

In contrast to the multiphase multilayer oxidation products just described for polished samples, abraded specimens of alloy I show much lower kinetics (Fig. 1) and Cr_2O_3 as the predominant oxidation product at 1000°C. Oxidation at this temperature was carried out for up to 26 hr duration, and only traces of NiO or spinel were detected. Microprobe scans taken from the 26-hr exposure specimen are presented in Fig. 5. The oxide is observed to be 5 μ or less in thickness. One significant difference in these two preparation techniques is apparently associated with the relative depth of a deformed surface layer on the alloy. Studies[21,22] of the metallurgical effects of mechanical polishing and abrasion have concluded that the polishing step effectively removes the majority of the deformation layer produced during the earlier abrasion stages of preparation. Consequently, abraded samples contain a cold-worked surface region which is essentially absent on the polished samples.

The observed surface preparation effect during oxidation is not unusual since a number of other studies[14,23–25] have reported similar effects in Cr-containing alloys. Most investigators conclude that enhanced diffusion of Cr occurs in the cold-worked surface region, resulting in selective oxidation of Cr to form a protective Cr_2O_3 film. The rapid diffusion paths may be a

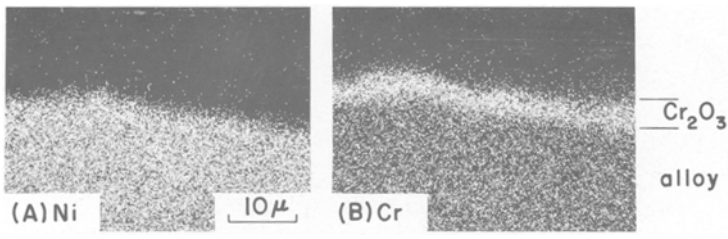

Fig. 5. Microprobe x-ray images taken from abraded specimen of Ni–13.5Cr–1ThO_2 following 26-hr exposure at 1000°C.

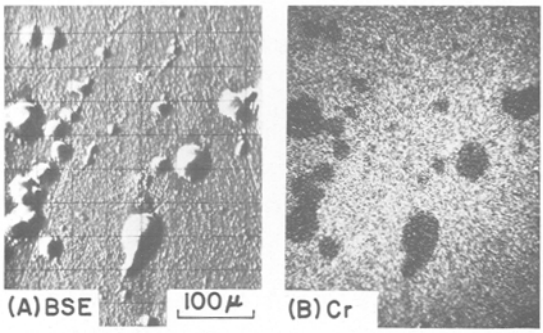

Fig. 6. Oxidation of abraded specimen of Ni–13.5Cr–1ThO_2 for 5 min at 1200°C. (a) Microprobe backscattered electron image. (b) Cr x-ray image; mounds of NiO are initiating subsequent to Cr_2O_3 formation.

direct result of the high dislocation density or they may be associated with the significant increase in grain boundary density accompanying recrystallization of the deformed region. The latter case has been shown to occur in Ni–Cr alloys.[14]

At 1200°C, x-ray diffraction results show that while Cr_2O_3 does form initially on abraded specimens, within a few minutes NiO begins to form and replace Cr_2O_3 as the external scale. This phenomenon is illustrated in Fig. 6 for an abraded specimen of alloy I oxidized for 5 min. The microprobe backscattered electron images of the alloy surface [Fig. 6(a)] reveal mounds of NiO which have been initiated at discrete points on the surface which is otherwise covered with a thin layer of Cr_2O_3. The x-ray image for Cr in Fig. 6(b) shows a high Cr concentration for the Cr_2O_3 portion of the oxide, while the areas of low Cr indicate NiO formation. The NiO formation, as determined from x-ray and optical results, is not easily discernable on a corresponding x-ray image for Ni, since the thin Cr_2O_3 layer does not prevent detection of the Ni radiation from the underlying alloy.

The subsequent initiation and growth of NiO to replace the initially formed Cr_2O_3 at 1200°C occurred at differing rates on the two sides of the alloy. This is a direct consequence of the variation in Cr content across the thickness of the alloy. On the lower Cr content side of the coupon, the duplex-type NiO scale had engulfed the entire surface within the first hour of exposure. In contrast, the higher Cr side of the coupon still retained some small areas of Cr_2O_3 after as much as 50 hr of exposure. Variations such as this led to the simultaneous measurement of several rate processes, making quantitative interpretation difficult. Such variations also emphasize that

13.5% Cr is approximately the critical value of Cr required for selective oxidation on these thoriated alloys at 150 Torr oxygen pressure.

A qualitative description of the kinetic behavior for abraded specimens of alloy I at 1200°C is derived from examination of scale morphologies at various reaction times. A thin layer of Cr_2O_3 forms over the entire specimen initially, producing much lower weight gains than for polished specimens which formed NiO at the start of the oxidation exposure. However, within the first few hours of exposure, the growth of NiO becomes appreciable and causes the onset of the rapid weight gain period shown in Fig. 1. The sequence of oxidation reactions under these conditions is observed to have a pronounced detrimental effect on the formation of a Cr_2O_3 continuous subscale beneath the NiO. Following 26 hr of exposure, the specimen contains very few areas where the continuous subscale has formed. Examination of sectioned specimens revealed a continuous band of internal oxidation particles in the alloy adjacent to the NiO scale, as shown in Fig. 7. The failure of the Cr_2O_3 healing layer to form and the continued growth of the NiO scale accounts for the eventual weight increase over that of the polished specimens, where the healing layer formed within a few hours.

The simultaneous growth of NiO and Cr_2O_3 as the external scale on adjacent areas of the alloy surface affords a convenient comparison between the characteristics of these two scales. Figure 8 illustrates this comparison in a photomicrograph taken under polarized light illumination. The duplex-type NiO scale is clearly observed in region A, while region B is covered with a thin layer of Cr_2O_3, which has subsequently spalled from the alloy during cooling. Electron microprobe line traces for Ni and Cr across each region are also illustrated in Fig. 8. As pointed out previously, the outer portion of the duplex NiO contains a small amount of Cr, while the inner layer has a Cr content in excess of that in the underlying alloy. This Cr distribution in the inner layer is illustrated as a smooth profile, but the microprobe trace

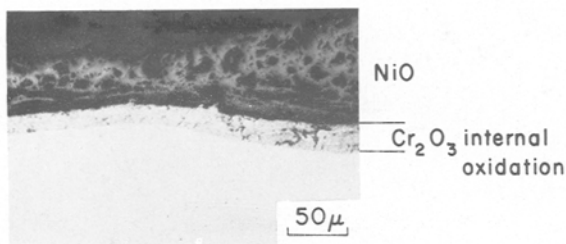

Fig. 7. Oxide scale morphology for abraded specimen of Ni–13.5Cr–1ThO_2 following 26-hr exposure at 1200°C. A layer of internal oxidation particles (Cr_2O_3) exists beneath NiO.

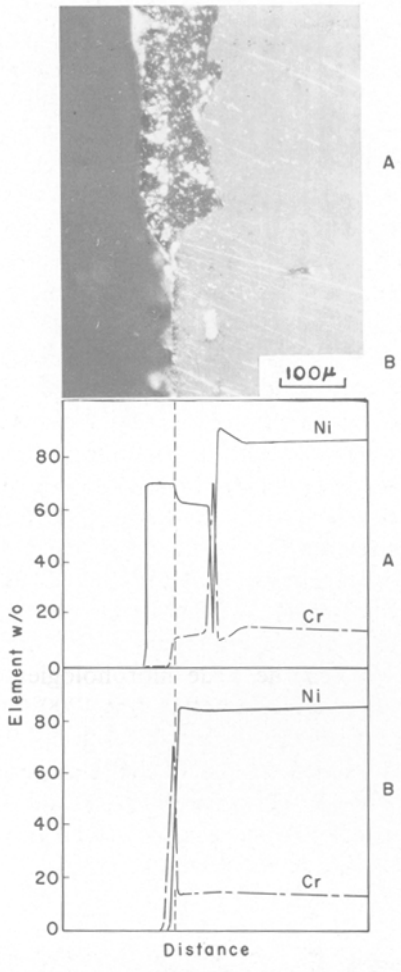

Fig. 8. Polarized light micrograph showing growth of NiO and Cr_2O_3 as the external scale on adjacent areas of specimen. Concentration profiles for Ni and Cr are shown across both areas.

showed an irregular profile, corresponding to small, discrete $NiCr_2O_4$ and Cr_2O_3 particles distributed throughout the inner layer. An additional feature which is revealed by the concentration profiles in Fig. 8 is the formation of a Cr depletion zone in the alloy beneath the oxide. In this sample, the depletion of Cr is more pronounced beneath the NiO than beneath the Cr_2O_3 external scale.

An analysis of the alloy compositional changes which occur during selective oxidation has been carried out by Whittle *et al.*[26] Following initial oxide formation, a large decrease in the solute concentration occurs in the alloy adjacent to the oxide–alloy interface, producing a steep concentration gradient. If a protective oxide is formed, an increase in oxidation time decreases this concentration gradient and increases the depth of depletion of the solute. A corresponding increase in solute concentration at the alloy–oxide interface occurs. Applying this analysis to the results in Fig. 8, the differences in the concentration profiles can be rationalized. The NiO duplex scale formation (containing Cr_2O_3 particles) can be considered to produce no significant Cr depletion in the alloy since both Ni and Cr are being consumed. Appreciable Cr depletion results from the subsequent formation of a continuous subscale, which develops following several hours of exposure. In comparison, a sharp Cr concentration gradient is established beneath the Cr_2O_3 external scale at the beginning of the oxidation exposure. Consequently, alloy regions beneath the NiO duplex scale have experienced less time, as compared to areas beneath the Cr_2O_3 external scale, to decrease the concentration gradient of Cr.

Figure 9 shows x-ray images for Ni and Cr taken over the same area as that shown in Fig. 8. The same features relating to Fig. 8 are again enumerated here.

A comparison between the scale morphologies of NiO and Cr_2O_3 formed on an abraded specimen of alloy I at 1200°C is shown in Fig. 10. The low magnification scanning electron micrograph [Fig. 10(a)] exhibits a region where the NiO and Cr_2O_3 join, while the high magnification micrographs [Figs. 10(b) and 10(c)] illustrate NiO and Cr_2O_3, respectively. The NiO grains are observed to be in excess of 10 μ average dimension while the Cr_2O_3 particles are less than 1 μ average size.

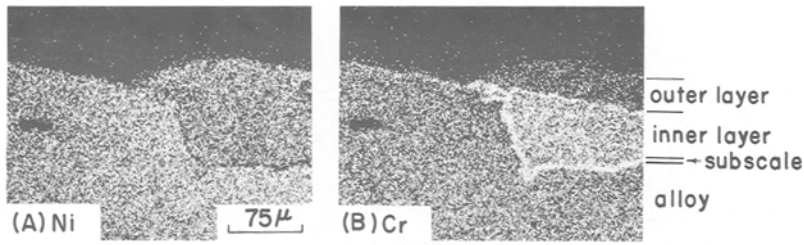

Fig. 9. Microprope x-ray images across identical area shown in Fig. 8. Abraded specimen of Ni–13.5Cr–1ThO_2 oxidized for 46 hr at 1200°C.

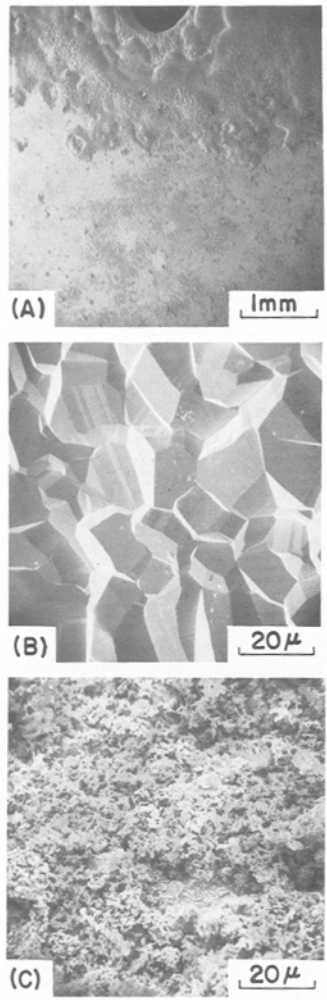

Fig. 10. (a) Surface morphology of abraded specimen of Ni–13.5Cr–1ThO_2 following 46-hr exposure at 1200°C. (b) NiO region. (c) Cr_2O_3 region.

Alloy II and Alloy III Oxidation Behavior

The oxidation characteristics of Ni–22.6Cr–1ThO_2 and Ni–33.7Cr–1ThO_2 are discussed simultaneously since no significant difference in the behavior of these alloys was observed. Figures 11 and 12 illustrate the gravimetric behavior for alloy II and alloy III respectively. In each case, at 1200°C the alloy is observed to gain weight initially and reach a maximum after only a few hours of exposure. A linear rate of weight loss then occurs, corresponding to the loss of Cr_2O_3 (*s*) via the formation of CrO_3 (*g*).[27]

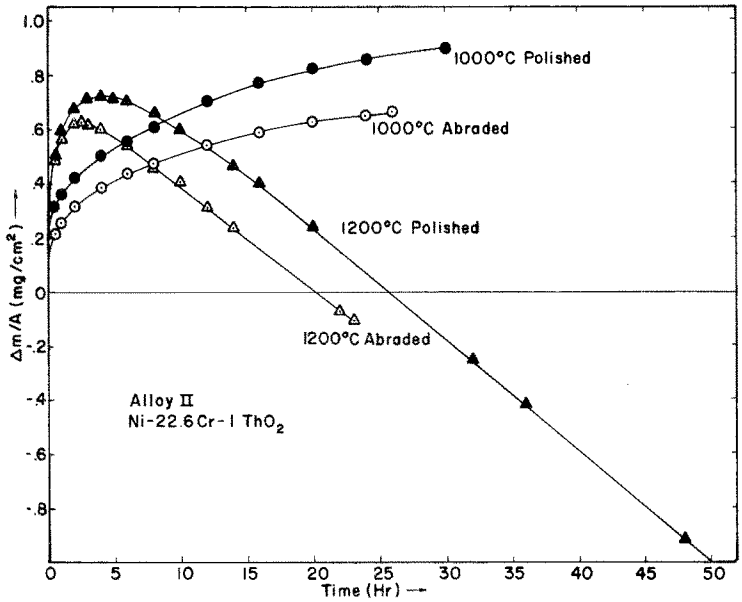

Fig. 11. Oxidation kinetics for Ni–22.6Cr–1ThO_2 at 1000 and 1200°C.

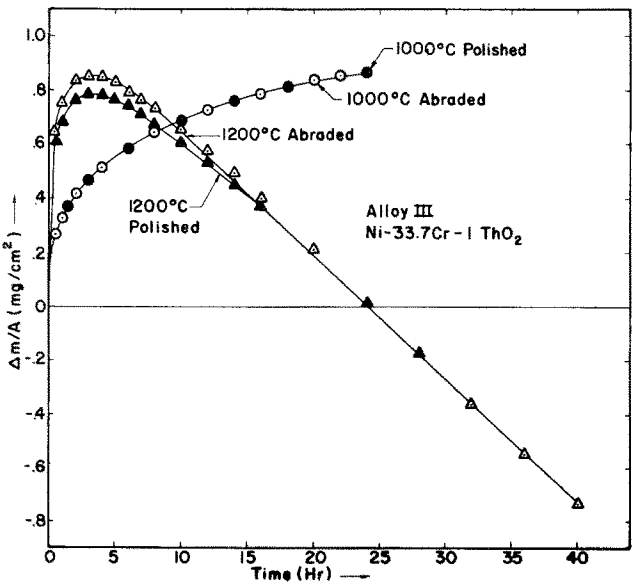

Fig. 12. Oxidation kinetics for Ni–33.7Cr–1ThO_2 at 1000 and 1200°C.

At 1000°C, reaction of the Cr_2O_3 with oxygen to form the vapor species CrO_3 is negligible compared to the rate of formation of Cr_2O_3, so that only weight gains are observed during oxidation.

Only minor differences in the weight change for abraded and polished specimens were observed for alloy II, although some differences in the oxidation products did occur. At both 1000 and 1200°C, as seen in Fig. 11, the polished samples gained more weight than the abraded ones. This small difference in the weight change is attributed to the fact that abraded specimens show only Cr_2O_3 as the oxidation product, while polished samples of alloy II show small amounts of spinel in addition to Cr_2O_3. The spinel occurs as a discontinuous, broken layer at the oxide–gas interface, outside of the continuous Cr_2O_3 scale. It is probable that NiO formed initially and was converted to spinel by solid-state reaction with Cr_2O_3 as the exposure time increased. Figure 13 shows the microprobe x-ray images for a polished sample oxidized at 1000°C for 30 hr. The predominant portion of the scale contains the high Cr concentration, i.e., Cr_2O_3, while the oxide region containing the Ni content appears outside the Cr_2O_3. The surface morphology of the oxide in this case is shown in the SEM micrograph in Fig. 14. This micrograph, taken of the surface of a polished sample of alloy II following 60 hr exposure at 1200°C, reveals a discontinuous scale of spinel at the external surface, with areas of the underlying Cr_2O_3 also being observed.

For alloy III, selective oxidation of Cr occurred on both polished and abraded samples, resulting in the formation of continuous Cr_2O_3 external scales. No NiO or spinel formation was detected by x-ray diffraction or microprobe scans. Consequently, the two surface preparation techniques produce no significant differences in the oxidation behavior (Fig. 12). Therefore, the agreement in the data for polished and abraded samples of alloy III essentially illustrates the reproducibility of the gravimetric data for alloys II and III.

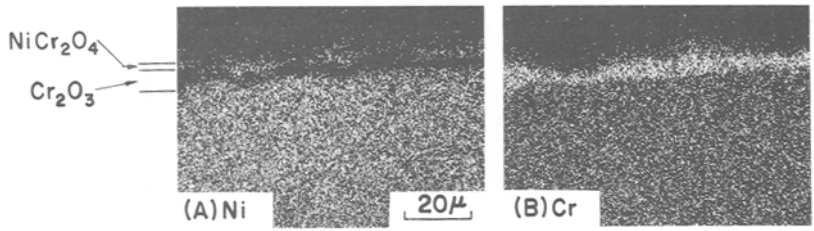

Fig. 13. Microprobe x-ray images taken from polished specimen of Ni–22.6Cr–1ThO_2 following 30-hr exposure at 1000°C.

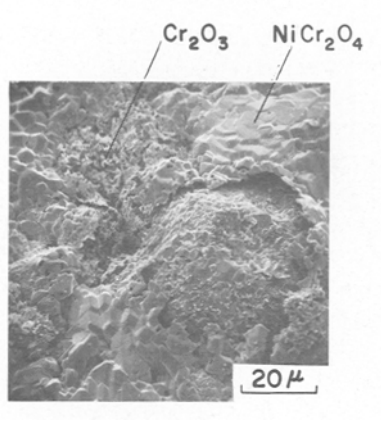

Fig. 14. External surface morphology of specimen shown in Fig. 13. Note discontinuous layer of $NiCr_2O_4$.

Both alloys II and III undergo selective oxidation of Cr at 1000 and 1200°C, resulting in the formation of Cr_2O_3 scales. Although alloy II forms some NiO or spinel initially when it is oxidized in the polished condition, this has been shown to be a thin, discontinuous outer scale. Consequently, the subsequent oxidation–vaporization of the Cr_2O_3 beneath it remains unaffected, as shown by the vaporization rates listed in Table I. These values are in excellent agreement with those reported earlier[27] for Cr_2O_3 pellets, indicating that the vaporization rates are not affected by the presence of ThO_2.

Table I. Vaporization Rate Constants (k_1) at 1200°C

Alloy (wt. % Cr)	Surface preparation	Oxide products	Exposure time (hr)	k_1 $\times 10^{-8}$ g/cm^2 · sec
22.6	Abraded	Cr_2O_3	23	1.1
22.6	Polished	Cr_2O_3	60	1.2
		Spinel discontinuous outer layer		
33.7	Polished	Cr_2O_3	28	1.2
		Spinel discontinuous outer layer		
33.7	Abraded	Cr_2O_3	41	1.3
33.7	Abraded	Cr_2O_3	45	1.1
33.7	Abraded	Cr_2O_3	148	1.0

For vaporization from Cr_2O_3 pellets, the electrobalance measures the rate of weight loss of Cr_2O_3 via the reaction

$$Cr_2O_3(s) + \tfrac{3}{2}O_2 \rightarrow 2\,CrO_3(g) \tag{1}$$

However, during alloy oxidation, a steady-state thickness of Cr_2O_3 is reached when the Cr_2O_3 formation rate becomes equal to the vaporization rate. At this point, the net amount of condensed oxide remains constant, and the electrobalance measures the rate at which Cr is removed from the alloy by forming $CrO_3(g)$. For the formation of an equal quantity of CrO_3 as in Eq. (1) (which should be the basis for comparison under identical experimental conditions), we have

$$2\,Cr + \tfrac{6}{2}O_2 \rightarrow 2\,CrO_3(g) \tag{2}$$

Thus, the vaporization rate which is measured during alloy oxidation [k_1 (alloy)] is related to that for the Cr_2O_3 pellet by

$$k_1\,(\text{alloy}) = (2M_{Cr}/M_{Cr_2O_3})/k_1(Cr_2O_3) \tag{3}$$

where M_{Cr} and $M_{Cr_2O_3}$ are atomic or molecular weights. Using the same experimental conditions as for the alloy oxidation tests, $k_1(Cr_2O_3)$ was found[27] at 1200°C to be 1.6×10^{-8} g/cm^2 · sec, or k_1 (alloy) $= 1.1 \times 10^{-8}$. This rate of vaporization corresponds to a linear recession rate of 0.2 mils/hr for one side of the alloy.

The Cr_2O_3 scales, which have been shown to occur under many conditions, are quite thin, generally being 5 μ or less in thickness. This, coupled with the fact that the initial ThO_2 content in the alloys is low (1 vol.%), produces difficulties in using microprobe techniques to detect if thorium is present in the Cr_2O_3 layers. However, when these oxidation results are compared to the behavior of similar unthoriated alloys, a distinct difference is observed, which may be related to the presence of ThO_2 in the alloy. For Ni–20Cr alloys, Cr_2O_3 external scales are reported[2,14] only in the region of alloy grain boundaries. In order to produce Cr_2O_3 external scales over the alloy grains, 30% Cr in Ni is required. However, selective oxidation of Cr has been shown to occur on alloy II in this study. Thus, enhanced Cr diffusion is again suggested for the thoriated alloys.

Giggins and Pettit[28] have reported that the parabolic rate constant for the growth of Cr_2O_3 on Ni–20Cr–2ThO_2 is approximately an order of magnitude smaller than that for the growth of Cr_2O_3 on Ni–30Cr. The oxidation rates observed in the present paper are in agreement with those reported for Ni–20Cr–2ThO_2. In general, Cr_2O_3 is considered[29–31] to be a metal-deficient *p*-type semiconductor, with the growth of Cr_2O_3 scales on Cr-containing alloys occurring by the outward diffusion of cations.[32] Using platinum marker experiments, both Giggins and Pettit[28] and Wallwork

and Hed[33] have concluded that the Cr_2O_3 scale on thoriated Ni–Cr grows inward. While results presented here are consistent with this conclusion, no satisfactory explanation to account for such a change in growth mechanism has yet been formulated.

The gravimetric results shown in Figs. 11 and 12 appear qualitatively to lend themselves to a paralinear type analysis. General treatments of this type are reported in the literature[34,35] and recently have been applied to the oxidation of a commercial thoriated Ni–Cr alloy.[28] In the present investigation, paralinear analyses of the data given in Figs. 11 and 12 were carried out, but the results were not satisfactory. A good quantitative description of the experimental data was not produced, primarily because the parabolic rate constants change with time. The large initial value of k_p decreases asymptotically to approach a steady-state value as oxidation of the alloy continues. Use of the k_p value calculated from the short-time oxidation yields a paralinear curve which fails to describe the extended oxidation behavior. Conversely, use of the steady-state k_p value in the paralinear analysis does not fit the initial weight-change results. Giggins and Pettit[28] encountered a similar variation in k_p with time, but attributed the large initial value to the small amount of NiO which formed during the early stages of oxidation. Although the NiO formation does contribute to the observed variation in k_p, it apparently is not solely responsible for this effect, since the oxidation product for alloy III is entirely Cr_2O_3, yet the k_p variation is analogous to that for the case where some NiO forms also. Assuming that a different growth mechanism is produced by the presence of the ThO_2 particles, a time-dependent change in the oxidation mechanism may occur. The k_p values corresponding to the initial stage of oxidation result from normal cation diffusion through the Cr_2O_3, and a subsequent gradual reduction in the oxidation rate occurs as the scale becomes "affected" by the ThO_2. A certain amount of justification exists for this description, since the k_p value for alloy III is 3.6×10^{-11} $g^2/cm^4 \cdot sec$ for the first 30 min of exposure at 1000°C, which is in excellent agreement with the rate constant reported[2] for Ni–30Cr.

SUMMARY AND CONCLUSIONS

The oxidation behavior of thoriated Ni–Cr alloys containing different Cr contents has been studied at 1000 and 1200°C. A compilation of the oxide scale compositions formed under various conditions is presented in Table II.

The fine grain substructure and associated dislocation density, which is stabilized by the ThO_2 particles, promotes short circuit Cr diffusion in these alloys. This enhanced Cr diffusivity is responsible for (1) the rapid formation

Table II. Oxides Formed on Ni–Cr–1ThO_2 Alloys

Alloy (wt.%Cr)	Temperature (°C)	Surface preparation	Exposure time (hr)	Oxide composition
13.5	1000	Abraded	26	Cr_2O_3 thin layer NiO, spinel trace amounts
		Polished	$\frac{1}{6}$	NiO duplex scale; Cr_2O_3, spinel small amounts; Cr_2O_3 internal oxidation
			16	NiO duplex scale Cr_2O_3, spinel small amounts Cr_2O_3 continuous subscale
	1200	Abraded	$\frac{1}{12}$	Cr_2O_3 thin layer NiO small amounts
			26	NiO duplex scale Cr_2O_3, spinel small amounts Cr_2O_3 internal oxidation
		Polished	21	NiO duplex scale; Cr_2O_3, spinel small amounts Cr_2O_3 continuous subscale
22.6	1000	Abraded	26	Cr_2O_3 thin layer
		Polished	30	Cr_2O_3 thin layer spinel discontinuous outer layer
	1200	Abraded	23	Cr_2O_3 thin layer
		Polished	60	Cr_2O_3 thin layer spinel discontinuous outer layer
33.7	1000	Abraded	22	Cr_2O_3 thin layer
		Polished	24	Cr_2O_3 thin layer
	1200	Abraded	$1\frac{1}{2}$	Cr_2O_3 thin layer
			148	Cr_2O_3 thin layer
		Polished	28	Cr_2O_3 thin layer

of continuous Cr_2O_3 subscales beneath a NiO duplex scale on Ni–13.5Cr–1ThO_2, and (2) selective oxidation of Cr on Ni–22.6Cr–1ThO_2.

For Ni–13.5Cr–1ThO_2, the oxidation mechanism is sensitive to specimen surface preparation, illustrating that 13.5 wt.% Cr is near the critical amount necessary to produce selective oxidation on these thoriated alloys.

For Ni–22.6Cr–1ThO_2, these and other results indicate that a change in growth mechanism occurs for Cr_2O_3, producing an order of magnitude reduction in oxide growth rate. Consequently, the formation of the vapor species CrO_3 becomes rate controlling after only a few hours of exposure at 1200°C.

ACKNOWLEDGMENTS

The authors express their thanks to B. A. Wilcox of Battelle Memorial Institute for supplying the alloys for this investigation and to Sherritt Gordon Mines Ltd. for permission to use the alloys. The authors gratefully thank W. C. Tripp, R. A. Rapp, and N. M. Tallan for their helpful discussions and critical review of the manuscript, and H. E. Leichty for technical assistance.

REFERENCES

1. B. A. Wilcox and A. H. Clauer, *Metal Sci. J.* **3**, 26–33 (1969).
2. C. S. Giggins and F. S. Pettit, *Trans. TME-AIME* **245**, 2495–2507 (1969).
3. R. A. Rapp, *Proc. 2nd Bolton Landing Conference on Oxide Dispersion Strengthening (1966)* (Gordon-Breach Publ., New York, 1969).
4. H. C. Graham, W. C. Tripp, and H. H. Davis, Microbalance techniques associated with oxidation studies, presented at Ninth Conference on Vacuum Microbalance Techniques, West Berlin, June 1970, in *Vacuum Microbalance Techniques*, Vol. 9 (Plenum Press, New York, to be published).
5. R. A. Rapp, *Corrosion* **21**, 382–400 (1965).
6. J. A. Sartell and C. H. Li, *J. Inst. Metals* **90**, 92–96 (1961–62).
7. N. Birks and H. Rickert, *J. Inst. Metals* **91**, 308–311 (1962–63).
8. J. Moreau and J. Benard, *Compt. Rend.* **237**, 1417–1419 (1953).
9. G. C. Wood and T. Hodgkiess, *Nature* **211** (5056), 1358–1361 (1966).
10. G. C. Wood and T. Hodgkiess, *J. Electrochem. Soc.* **113** (4), 319–327 (1966).
11. S. Mrowec and T. Werber, *J. Electrochem. Soc.* **105** (6), 363 (1958).
12. F. S. Pettit and E. J. Felton, *J. Electrochem. Soc.* **111** (2), 135–139 (1964).
13. P. K. Kofstod and A. Z. Hed, *J. Electrochem. Soc.* **116** (2), 224–234 (1969).
14. C. S. Giggins and F. S. Pettit, *Trans. TME-AIME* **245**, 2509–2514 (1969).
15. D. L. Douglass, *Corrosion Sci.* **8**, 665–678 (1968).
16. I. A. Kvernes and H. H. Davis, to be published.
17. I. A. Kvernes, H. H. Davis, and H. C. Graham, to be published.
18. M. J. Fleetwood, *J. Inst. Metals* **94**, 218–223 (1966).
19. D. A. Jones and R. E. Westerman, *Corrosion* **21**, 295–305 (1965).
20. H. H. Davis and H. C. Graham, unpublished.
21. E. Rabinowicz, *Sci. Am.* **218**, 91–99 (1968).
22. L. E. Samuels, *Metallurgia* **66** (396), 187–199 (1962).
23. M. Warzee, J. Hennant, M. Mauric, C. Sohen, and J. Waty, *J. Electrochem. Soc.* **112** (7), 670–674 (1965).
24. G. Ostberg, L. Unneberg, M. de Pourbaix, S. Janssen, W. Hubner, and L. Hammar, *Trans. Am. Nucl. Soc.* **8**, 122 (1965).
25. J. Poulignier, *Corrosion et Anti-Corrosion* **11**, 463 (1963).
26. D. P. Whittle, D. J. Evans, D. B. Scully, and G. C. Wood, *Acta Met.* **15**, 1421–1430 (1967).
27. H. C. Graham and H. H. Davis, *J. Am. Ceram. Soc.* **54** (2), 89 (1971).
28. C. S. Giggins and F. S. Pettit, *Met. Trans.* **2**, 1071–1078 (1971).
29. W. C. Hagel and A. U. Seybolt, *J. Electrochem. Soc.* **108** (12), 1146–1152 (1961).
30. J. A. Crawford and R. W. Vest, *J. Appl. Phys.* **35**, 2413–2424 (1964).
31. L. C. Walters and R. E. Grace, *J. Appl. Phys.* **36**, 2331–2332 (1965).
32. G. C. Wood and D. P. Whittle, *J. Electrochem. Soc.* **115** (2), 126–133 (1968).
33. G. R. Wallwork and A. Z. Hed, *Oxidation of Metals* **3**, 229 (1971).
34. E. W. Haycock, *J. Electrochem. Soc.* **106** (9), 771–775 (1959).
35. C. S. Tedmon, Jr., *J. Electrochem. Soc.* **113** (9), 766–768 (1966).